Supporting Information for "Top-of-atmosphere albedo bias from neglecting three-dimensional radiative transfer through clouds"

Clare E. Singer[1], Ignacio Lopez-Gomez[1], Xiyue Zhang[1] *, Tapio Schneider[1,2]

[1]Department of Environmental Science and Engineering, California Institute of Technology, Pasadena, California, USA.

[2]Jet Propulsion Laboratory, California Institute of Technology, Pasadena, California, USA.

Contents of this file

1. Text 1 to 4
2. Figures S1 to S2

Introduction The supplement includes four sections. In the first section, there is detailed information about the large-eddy simulation (LES) code PyCLES that was used to generate the three-dimensional cloud fields used in this study. Details about each of the four LES cases are also provided. The second section includes details about the libRadtran

Corresponding author: C. E. Singer, Department of Environmental Science and Engineering, California Institute of Technology, MC C1-221, Pasadena, CA 91125, USA. (csinger@caltech.edu)

*Current affiliation: National Center for Atmospheric Research, Boulder, CO, USA.

code and MYSTIC radiative transfer solver as well as microphysical assumptions. The third and fourth sections document dependence of the results in the main text on the ice crystal parameterization and LES resolution, respectively.

1. LES model setup

LES are performed using the anelastic fluid solver PyCLES (Pressel et al., 2015). Subgrid-scale fluxes are treated implicitly by the WENO scheme used in the numerical discretization of the equations (Pressel et al., 2017).

For each case, the characteristic timescale of convection is evaluated and taken to be representative of the dynamical decorrelation time τ. Snapshots are taken at least one dynamical decorrelation time apart, so that the cloud samples can be treated as independent in a statistical analysis of the flux biases. The decorrelation timescale is calculated as

$$\tau = \frac{z_{bl}}{w^*} + \frac{d_c}{\bar{w}_u}, \tag{1}$$

where z_{bl} is the mixed-layer height, $w^* = \left(z_{bl}\, \overline{w'b'}\Big|_s\right)^{1/3}$ is the Deardoff convective velocity, d_c is the cloud depth, and $\bar{w}_u$ is the mean updraft velocity within the cloud.

1.1. Shallow cumulus (ShCu) convection, BOMEX

The BOMEX LES case study is described in Siebesma et al. (2003). Surface boundary conditions, $\overline{w'q_t'}|_s$ and $\overline{w'\theta_l'}|_s$ are prescribed, resulting in sensible and latent heat fluxes of about 10 and 130 W m^{-2}, respectively. The atmospheric column is forced by clear-sky longwave radiative cooling, neglecting radiative cloud effects. A prescribed subsidence profile induces mean vertical advection of all fields, and specific humidity is further forced

by large-scale horizontal advective drying in the lower 500 m. The liquid-water specific humidity is diagnosed through a saturation adjustment procedure. For BOMEX, the characteristic timescale of convection is $\tau \approx 40$ min, where $z_{bl} = 500$ m, $w^* = 0.66$ m s^{-1}, $d_c = 1300$ m, and $\bar{w}_u = 0.85$ m s^{-1}, and snapshots are taken every 1 hour. The domain size is set to 6.4 km in the horizontal and 3 km in the vertical. Results are reported for an isotropic resolution of $\Delta x_i = 20$ m.

1.2. Shallow cumulus (ShCu) convection, RICO

The RICO LES case study is described in vanZanten et al. (2011). The surface sensible and latent heat fluxes are modeled using bulk aerodynamic formulae with drag coefficients as specified in vanZanten et al. (2011), resulting in fluxes of around 6 and 145 W m^{-2}, respectively. The atmospheric column is forced by prescribed profiles for subsidence and large-scale heat and moisture forcings that are a combination of radiative and advective forcings. A two-moment cloud microphysics scheme from Seifert and Beheng (2006) is used with cloud droplet concentration set to $N_d = 70$ cm^{-3}. For RICO, the characteristic timescale of convection is $\tau \approx 50$ min, where $z_{bl} \approx 500$ m, $w^* \approx 0.62$ m s^{-1}, $d_c = 2500$ m, and $\bar{w}_u \approx 1.2$ m s^{-1}, and snapshots are taken every 1 hour. The domain size is set to 12.8 km in the horizontal and 6 km in the vertical. Results are reported for an isotropic resolution of $\Delta x_i = 40$ m.

1.3. Stratocumulus-topped marine boundary layer (Sc), DYCOMS-II RF01

The simulation setup for DYCOMS-II RF01 follows the configuration of Stevens et al. (2005). The initial state consists of a well-mixed layer topped by a strong inversion in temperature and specific humidity, with $\Delta\theta_l = 8.5$ K and $\Delta q_t = -7.5$ g kg^{-1}. Surface

latent and sensible heat fluxes are prescribed as 115 and 15 W m^{-2}, respectively. In addition, the humidity profile induces radiative cooling above cloud-top and warming at cloud-base. As in BOMEX, the liquid-water specific humidity is diagnosed through a saturation adjustment procedure. For the stratocumulus clouds, without strong updrafts and a thin cloud layer, the characteristic convective timescale is taken to be just the first term of Equation (1), which evaluates to $\tau \approx 20$ min, with $z_{bl} = 850$ m and $w^* = 0.8$ m s^{-1}. Snapshots taken every 30 minutes are used in the analysis. The domain size is set to 3.36 km in the horizontal and 1.5 km in the vertical. Results are reported for a resolution of $\Delta z = 5$ m in the vertical and $\Delta x = 35$ m in the horizontal.

1.4. Deep convection (Cb), TRMM-LBA

Deep convective clouds are generated using the TRMM-LBA configuration detailed in Grabowski et al. (2006), based on observations of the diurnal cycle of convection in the Amazon during the rainy season. The diurnal cycle is forced by the surface fluxes, which are prescribed as a function of time. The magnitude of the fluxes maximizes 5.25 hours after dawn, with a peak latent and sensible heat fluxes of 554 and 270 W m^{-2}, respectively. The radiative cooling profile is also prescribed as a function of time. We use the one-moment microphysics scheme based on Kaul, Teixeira, and Suzuki (2015) with modifications described in Shen, Pressel, Tan, and Schneider (2020). Since this case study is not configured to reach a steady state, the simulation is run up to $t = 7$ hours. Deep convection is considered to be fully developed after 5 hours, when the liquid-water and ice-water paths stabilize (Grabowski et al., 2006). The ensemble of cloud snapshots is formed by sampling at $t = 7$ hours from a set of simulations with different initial conditions.

The random perturbations used in the initialization ensure that all cloud snapshots in the ensemble are uncorrelated. The domain size is set to 20 km in the horizontal and 22 km in the vertical. Results are reported for a resolution of $\Delta z = 50$ m in the vertical and $\Delta x = 100$ m in the horizontal.

2. libRadtran specifics

The MYSTIC solver from libRadtran requires three-dimensional fields of liquid and ice water content and particle effective radius as input. The LES uses bulk microphysics schemes and does not explicitly compute the effective radius. For liquid-only clouds, the parameterization from Ackerman et al. (2009) and Blossey et al. (2013) with assumed droplet number of $N_d = 10^8$ m^{-3} is used. The full Mie scattering phase function is taken from the libRadtran lookup tables. Because the lookup tables are only valid for droplets with radius greater than 1 μm, smaller calculated effective radii were rounded to this minimum value.

For ice clouds, the parameterization from Wyser (1998) is used. The `hey` parameterization from Yang et al. (2013) and Emde et al. (2016) with habit type set to `ghm` (general habit mixture) is used. The `hey` parameterization uses the full Mie phase function and does not employ the Henyey-Greenstein approximation which has been shown to be another source of error in radiative transfer (RT) (Barker et al., 2015). The results are not dependent on the exact choice for ice crystal shape or roughness (Figure S1). Note that the `hey` ice parameterization is only valid for radii less than 90 μm, and larger calculated effective radii were rounded to this maximum value.

The MYSTIC RT calculations are done using 10^4 photons sampled from the `kato2` correlated-k parameterization of the solar spectrum (Kato et al., 1999; Mayer & Kylling, 2005). The surface albedo was set to $\alpha_s = 0.06$.

3. Ice particle parameterization dependence

Deep convective clouds, reaching upwards of 10 km, nearly always contain ice crystals in addition to liquid water. Optical properties of ice crystals depend on their size, shape (or habit), and surface smoothness. Two different parameterizations, with three and four habit choices, respectively, were tested. The differences between these parameterization variants is negligible; it is much smaller than the variability stemming from the cloud dynamics (statistical spread between snapshots) and also much smaller than the magnitude of the 3D effects (Figure S1).

The `hey` parameterization with general habit mixture (`ghm`) is used in the main text (Yang et al., 2013; Emde et al., 2016). This parameterization is valid for a spectral range from $0.2 - 5\mu$m, and for ice effective radii from $5 - 90\mu$m. `hey` assumes smooth crystals and allows for four choices of habit: `ghm`, solid column (`col`), rough aggregate (`agg`), and `plate`.

The other parameterization tested was `baum_v36` (Heymsfield et al., 2013; Yang et al., 2013; Baum et al., 2014). This parameterization is valid over a wider spectral range ($0.2 - 99\mu$m), but a narrower effective radius range ($5 - 60\mu$m). Particles with effective radius outside of the accepted range were rounded to the maximum allowed value. The `baum_v36` parameterization assumes severely roughened particles. It allows for three choices of habit: `ghm`, solid column (`col`), and rough-aggregate (`agg`).

These seven variants are compared in Figure S1 for one cloud snapshot from the TRMM-LBA case and they show very similar results. Shown is both the absolute TOA reflected flux for the independent pixel approximation (IPA) and 3D RT and also the flux bias (IPA – 3D).

Also shown in Figure S1 is a RT calculation done on the same cloud field, but only including the liquid droplets and ignoring the ice particles. We use the full Mie scattering phase function without any parameterization for the liquid portion of the cloud in all cases. The difference between the liquid-only and liquid + ice TOA fluxes can be up to 20% depending on the parameterization used, but the flux bias (IPA - 3D) is very similar for the liquid-only and all ice parameterizations.

4. Resolution dependence

To test the resolution dependence of these results, the 3D fields from LES were interpolated to new grids at coarser resolution and the RT calculations were repeated on these coarse-grained grids. This regridding prevents changes in the cloud dynamics due to the resolution, and focuses on the resolution dependence of the RT by beginning with the same high-resolution LES output. First, the resolution was decreased isotropically by factors of 2, 4, and 8. Additionally, the resolution was decreased anisotropically, with $\Delta x = \Delta y$ increased by factors of 2 – 32, such that the aspect ratio was closer to that of an Earth system model (ESM).

The mean flux bias (1D−3D) as a function of solar zenith angle is shown in Figure S2 for the four cloud regimes and different resolutions. As shown, the resulting flux biases due to the IPA are robust across the resolutions considered.

References

Ackerman, A. S., VanZanten, M. C., Stevens, B., Savic-Jovcic, V., Bretherton, C. S., Chlond, A., ... Zulauf, M. (2009). Large-eddy simulations of a drizzling, stratocumulus-topped marine boundary layer. *Monthly Weather Review*, *137*(3), 1083–1110. doi: 10.1175/2008MWR2582.1

Barker, H. W., Cole, J. N. S., Li, J., Yi, B., & Yang, P. (2015). Estimation of Errors in Two-Stream Approximations of the Solar Radiative Transfer Equation for Cloudy-Sky Conditions. *Journal of the Atmospheric Sciences*, *72*(11), 4053–4074. doi: 10 .1175/JAS-D-15-0033.1

Baum, B. A., Yang, P., Heymsfield, A. J., Bansemer, A., Cole, B. H., Merrelli, A., ... Wang, C. (2014). Ice cloud single-scattering property models with the full phase matrix at wavelengths from 0.2 to 100um. *Journal of Quantitative Spectroscopy and Radiative Transfer*, *146*, 123–139. doi: 10.1016/j.jqsrt.2014.02.029

Blossey, P. N., Bretherton, C. S., Zhang, M., Cheng, A., Endo, S., Heus, T., ... Xu, K.-M. (2013). Marine low cloud sensitivity to an idealized climate change: The CGILS LES intercomparison. *Journal of Advances in Modeling Earth Systems*, *5*(2), 234–258. doi: 10.1002/jame.20025

Emde, C., Buras-Schnell, R., Kylling, A., Mayer, B., Gasteiger, J., Hamann, U., ... Bugliaro, L. (2016). The libRadtran software package for radiative transfer calculations (version 2.0.1). *Geoscientific Model Development*, *9*(5), 1647–1672. doi: 10.5194/gmd-9-1647-2016

Grabowski, W. W., Bechtold, P., Cheng, A., Forbes, R., Halliwell, C., Khairoutdinov,

M., ... Xu, K.-M. (2006). Daytime convective development over land: A model intercomparison based on LBA observations. *Quarterly Journal of the Royal Meteorological Society*, *132*(615), 317–344. doi: 10.1256/qj.04.147

Heymsfield, A. J., Schmitt, C., Bansemer, A., Heymsfield, A. J., Schmitt, C., & Bansemer, A. (2013). Ice cloud particle size distributions and pressure-dependent terminal velocities from in situ observations at temperatures from 0° to -86°C. *Journal of the Atmospheric Sciences*, *70*(12), 4123–4154. doi: 10.1175/JAS-D-12-0124.1

Kato, S., Ackerman, T. P., Mather, J. H., & Clothiaux, E. E. (1999). The k-distribution method and correlated-k approximation for a shortwave radiative transfer model. *Journal of Quantitative Spectroscopy and Radiative Transfer*, *62*(1), 109 - 121. doi: https://doi.org/10.1016/S0022-4073(98)00075-2

Kaul, C. M., Teixeira, J., & Suzuki, K. (2015). Sensitivities in Large-Eddy Simulations of Mixed-Phase Arctic Stratocumulus Clouds Using a Simple Microphysics Approach. *Monthly Weather Review*, *143*(11), 4393–4421. doi: 10.1175/MWR-D-14-00319.1

Mayer, B., & Kylling, A. (2005). Technical note: The libRadtran software package for radiative transfer calculations - description and examples of use. *Atmospheric Chemistry and Physics*, *5*(7), 1855–1877. doi: 10.5194/acp-5-1855-2005

Pressel, K. G., Kaul, C. M., Schneider, T., Tan, Z., & Mishra, S. (2015). Large-eddy simulation in an anelastic framework with closed water and entropy balances. *Journal of Advances in Modeling Earth Systems*, *7*(3), 1425–1456. doi: 10.1002/2015MS000496

Pressel, K. G., Mishra, S., Schneider, T., Kaul, C. M., & Tan, Z. (2017). Numerics and subgrid-scale modeling in large eddy simulations of stratocumulus clouds. *Journal of*

Advances in Modeling Earth Systems, *9*(2), 1342–1365. doi: 10.1002/2016MS000778

Seifert, A., & Beheng, K. D. (2006). A two-moment cloud microphysics parameterization for mixed-phase clouds. Part 1: Model description. *Meteorology and Atmospheric Physics*, *92*(1-2), 45–66. doi: 10.1007/s00703-005-0112-4

Shen, Z., Pressel, K. G., Tan, Z., & Schneider, T. (2020). Statistically Steady State Large-Eddy Simulations Forced by an Idealized GCM: 1. Forcing Framework and Simulation Characteristics. *Journal of Advances in Modeling Earth Systems*, *12*(2). doi: 10.1029/2019MS001814

Siebesma, A. P., Bretherton, C. S., Brown, A., Chlond, A., Cuxart, J., Duynkerke, P. G., ... Stevens, D. E. (2003). A large eddy simulation intercomparison study of shallow cumulus convection. *Journal of the Atmospheric Sciences*, *60*(10), 1201–1219. doi: 10.1175/1520-0469(2003)60⟨1201:ALESIS⟩2.0.CO;2

Stevens, B., Moeng, C.-H., Ackerman, A. S., Bretherton, C. S., Chlond, A., de Roode, S., ... Zhu, P. (2005). Evaluation of large-eddy simulations via observations of nocturnal marine stratocumulus. *Monthly Weather Review*, *133*(6), 1443–1462. doi: 10.1175/MWR2930.1

vanZanten, M. C., Stevens, B., Nuijens, L., Siebesma, A. P., Ackerman, A. S., Burnet, F., ... Wyszogrodzki, A. (2011). Controls on precipitation and cloudiness in simulations of trade-wind cumulus as observed during RICO. *Journal of Advances in Modeling Earth Systems*, *3*(2). doi: 10.1029/2011MS000056

Wyser, K. (1998). The effective radius in ice clouds. *Journal of Climate*, *11*(7), 1793–1802. doi: 10.1175/1520-0442(1998)011⟨1793:TERIIC⟩2.0.CO;2

Yang, P., Bi, L., Baum, B. A., Liou, K.-N., Kattawar, G. W., Mishchenko, M. I., ... Cole, B. (2013). Spectrally consistent scattering, absorption, and polarization properties of atmospheric ice crystals at wavelengths from 0.2 to 100 um. *Journal of the Atmospheric Sciences*, *70*(1), 330–347. doi: 10.1175/JAS-D-12-039.1

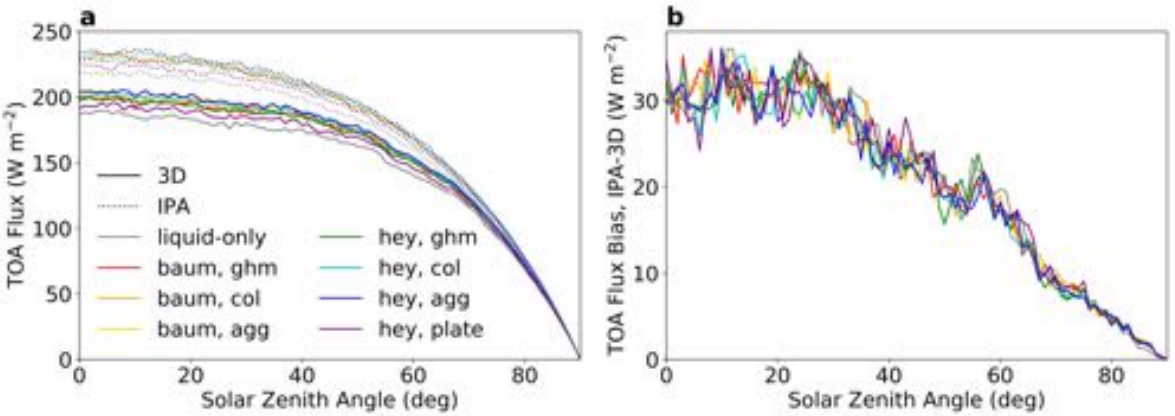

Figure S1. TOA reflected fluxes across zenith angles for different ice parameterizations in one TRMM-LBA cloud snapshot. (a) 3D and IPA fluxes. (b) Flux bias (IPA – 3D).

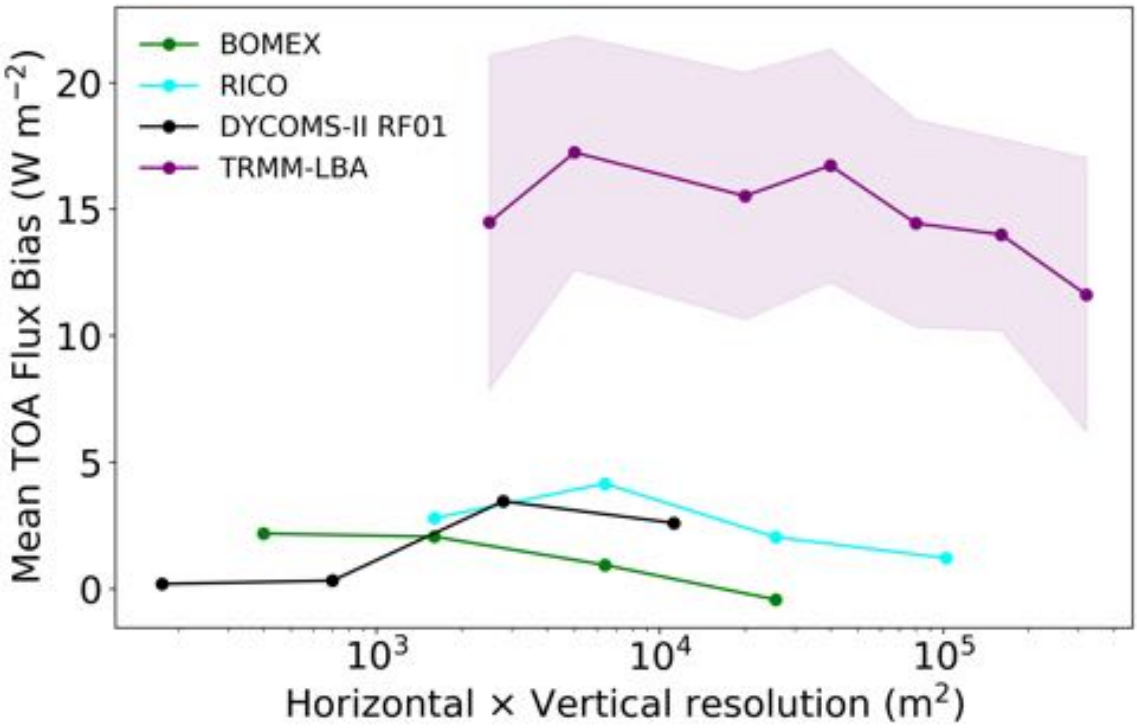

Figure S2. Mean TOA reflected flux bias across all solar zenith angles computed for different resolutions of the same cloud fields. The x-axis shows the resolution as the product of the horizontal and vertical resolutions in m^2, but the resolution was not decreased isotropically. The four cases of ShCu, Sc, and Cb are shown. For TRMM-LBA, because the spread across snapshots of the flux bias is so large, five snapshots are averaged together and the standard deviation is shown in the shading.